Binding of Calcium Ions to an Avian Flight Muscle Troponin T[†]

Zhiling Zhang,[‡] Jian-Ping Jin,[§] and Douglas D. Root*,[‡]

Department of Biological Sciences, Division of Biochemistry, University of North Texas, Denton, Texas 76203-5220 and Department of Physiology and Biophysics, Case Western Reserve University School of Medicine, 10900 Euclid Avenue, Cleveland, Ohio 44106-4970

Received June 20, 2003; Revised Manuscript Received December 15, 2003

ABSTRACT: Numerous troponin T (TnT) isoforms are generated by alternative RNA splicing primarily in its N-terminal hypervariable region, but the functions of these isoforms are not completely understood. Here for the first time, we discovered that a chicken fast TnT isoform with a unique Tx motif $(HEEAH)_n$ binds calcium. The metal binding behavior of this TnT isoform was first investigated using terbium as a calcium analogue due to its more readily detectable fluorescence variation upon TnT binding. Both intact TnT and TnT N-terminal fragment (TnT N47) bound terbium with high affinity indicating that the N-terminal sequence was the site of binding. Since terbium often substitutes at calcium-binding sites, radioactive calcium was tested and found to bind both intact TnT and TnT N47. Fluorescence measurements using the calcium-sensitive fluorescent dye, calcium green 5N, confirmed that calcium bound to the tertiary complex of TnT and the tropomyosin dimer with a fast on-rate (10^6-10^7 M^{-1} s^{-1}) as detected in stopped-flow analysis. Consistent with these observations, computational predictions suggest that TnT N47 might fold into an elongated structure with at least one high-affinity metal ion binding pocket comprised primarily of the Tx motif sequence and several lower affinity binding sites. These results suggest that TnT may play a role in modulating the calcium-mediated regulatory process of striated muscle contraction.

Troponin T (TnT)[1] is the tropomyosin (Tm)-binding subunit of the troponin complex and plays an essential role in the thin-filament regulatory system of vertebrate striated muscle. On its C-terminal domain, TnT interacts with troponin C (TnC), troponin I (TnI), Tm, and actin during Ca^{2+}-dependent regulation of muscle contraction (*1*−*3*) and is required for the Ca^{2+} sensitivity of myofibrillar ATPase. While the central portion of the elongated TnT structure is involved in Tm binding, less well understood is the N-terminal region and its variety of sequence variations.

TnT exhibits more diversity from alternative splicing than any other thin filament protein, and exists in multiple isoforms in different species, muscle fiber types, and developmental stages (*4*−*9*). Chicken fast skeletal muscle TnT is encoded by a single gene and expressed as many isoforms, which are produced by alternative splicing of the more than thirteen 5′-exons encoding the hypervariable N-terminal region and mutually exclusive splicing of two 3′-exons encoding a C-terminal variable region (*4*, *10*−*11*). Adult chicken TnT in breast and leg muscle are distinguished by their molecular mass and isoelectric points (pI) resulting from a dramatic difference in the N-terminal region (*10*, *12*). The major isoform of chicken breast muscle TnT has a molecular mass of 33 500 kDa and a pI of about 7, whereas the leg muscle isoforms have a molecular mass of about 30 500 kDa and a pI of about 8.5 (*13*). Although numerous TnT isoforms generated from alternative splicing have been investigated, the functional significance of this hypervariable region has not been well understood.

Sequencing of both chicken breast muscle TnT cDNA (*4*) and protein (*10*) showed a segment consisting of four repeated histidine pairs [H(E/A)EAH], named Tx sequence).

[†] The authors gratefully acknowledge support by grants from NIH, National Institute of Arthritis and Musculoskeletal and Skin Diseases (AR044737 to D.D.R. and AR048816 to J.-P.J.), and the American Heart Association (to D.D.R.).

* To whom correspondence should be addressed.

[‡] University of North Texas.

[§] Case Western Reserve University School of Medicine.

[1] Abbreviations: *B*, the concentration of Ca^{2+} bound to protein or calcium green 5N; *C*, the concentration of free Ca^{2+}; *c*, the ratio between *D* and I_0; *D*, the concentration of free calcium green 5N; D_T, the concentration of total calcium green 5N; d*C*/d*t*, the derivative of concentration with respect to time; DTT, dithiothreitol; EC50, the effective concentration of ligand when the bound ligand concentration equals 50% of the protein concentration; EDTA, ethylenediamine tetraacetic acid; EGTA ethylene glycol-bis(*β*-aminoethyl ether)-*N*,*N*,*N*′,*N*′-tetraacetic acid; FPLC, fast-purification liquid chromatography; GB/SA, generalized Born/surface area; HEDTA, hydroxyethyl ethylenediamine triacetic acid; *I*, the absolute difference in fluorescent intensity; I_0, the fluorescent intensity of free calcium green 5N; I_{Ca}, the fluorescent intensity of calcium green 5N when it binds Ca^{2+}; I_{max}, the maximum absolute difference in fluorescent intensity; *k*, the ratio between *B* and I_{Ca}; K_d, the apparent dissociation constant of ligand binding; k_{off}, the dissociation rate constant; k_{on}, the binding rate constant; mAb, monoclonal antibody; MMFF, the Merck molecular force field; OPLS-AA, optimized potentials for liquid simulations-all atom force field; *P*, protein concentration; P_T, the concentration of total protein; RMSD, root-mean-square deviation of the alpha carbons; SDS−PAGE, SDS−polyacrylamide gel electrophoresis; *T*, terbium concentration; Tm, tropomyosin; TnC, troponin C; TnI, troponin I; TnT, troponin T; TnT N47, N-terminal 46 amino acids of chicken breast muscle TnT1 isoform (residue 2−47); Tx cluster, the metal binding sequence of $[H(E/A)EAH]_n$.

10.1021/bi035067o CCC: $27.50
Published on Web 02/12/2004

The Tx sequence is largely encoded by alternatively spliced P exons between exon 5 and 6 (*11*), and has a highly organized structure in the adult breast muscle of two orders (*Galliformes* and *Craciforms*) of avian species (*14*). Because the expression of Tx and Tx-like sequence is specific to the adult avian pectoral muscle (*9*), a possible link has been implicated between this special N-terminal structure of TnT and the flight function of bird pectoral muscle. We have previously demonstrated specific binding of transition metal ions to the Tx structure (*14*). Studies on the Tx clusters using metal ion or monoclonal antibody binding to the N-terminal region demonstrated that the metal ion binding induces structural changes within the N-terminal Tx segment with secondary effects on the conformation and function of other domains of TnT (*15*−*16*). Further investigation using fluorescence spectral analysis revealed that the metal ion binding to the TnT N-terminus induces a conformational change in TnT together with a decrease in the mobility of the Trp residues (W234, W236, and W285) and an increase in the flexibility of fluorescein-labeled Cys_{263} in the COOH domain (*17*).

Studies on reconstituted thin filaments from the intact cardiac TnT and a TnT fragment with a deletion of the mainly acidic N-terminal 38 amino acids have demonstrated that removal of this TnT N-terminal peptide weakens TnC−Ca^{2+} binding thereby increasing the Ca^{2+} concentration required to activate the actin-myosin MgATPase (*18*). In addition, contractility studies using skinned adult chicken muscle fibers differing in the N-terminal Glu/Asp contents-determined overall charge of TnT (acidic breast verse basic levator coccygeus) showed that acidic TnT contributes to the function of the contractile apparatus by sensitizing force and stiffness responses to Ca^{2+} (*19*). Moreover, protein binding assays showed that TnT isoforms with a more acidic N-terminal domain had a higher tolerance to acidosis than did basic isoforms in TnI and Tm binding (*13*).

Previous investigations on the N-terminal structure of TnT indicate this region takes part in thin filament structure modulation (*17*). To better understand the function of TnT in Ca^{2+} regulation, the present study is the first direct test for the calcium binding to TnT in the N-terminal region. The calcium-binding test was first carried out by using terbium, an easily detectable calcium analogue. Then, radioactive calcium was used to trace the binding to different forms of TnT. We have shown that intact chicken breast muscle TnT and an N-terminal fragment (TnT N47) bind to calcium with similar affinity. Stopped-flow analysis using a calcium fluorescent dye showed that TnT−Tm binds to calcium with a fast on-rate. Molecular mechanics simulations further support the hypothesis that Tx motifs form Ca^{2+}-binding sites. These results suggest that the Glu-rich N-terminal region of chicken breast muscle TnT binds to calcium, and may play a role in modulating calcium regulation of muscle contraction.

EXPERIMENTAL PROCEDURES

Protein Preparation. Three forms of TnT were used in this research, TnT N47, the N-terminal 46 amino acids of chicken breast (fast) muscle TnT1 isoform (residues 2−47), chicken breast muscle TnT and reconstituted TnT−Tm complex. TnT N47 and chicken breast muscle TnT contain four and seven metal-binding Tx motifs (the sequence is presented in Figure 1), respectively, and were purified by Zn^{2+} affinity chromatography as previously demonstrated and quantified (*14*−*15*, *20*; see Supporting Information). TnT−Tm complex were reconstituted from chicken breast muscle TnT and rabbit skeletal muscle Tm, which was purified from acetone powder by the method of Smillie (*21*). To reconstitute TnT−Tm, chicken breast muscle TnT and rabbit skeletal muscle Tm were mixed in molar ratio of 1:2 and diluted with 15 mM Tris, 0.5 M NaCl, 1 mM DTT, 2 mM EDTA, and 6 M urea, pH 7.8 buffer. To renature the complex to native conformation, the mixture was dialyzed at 4 °C to remove urea and high salt gradually, to eventually reach the physiological condition of 15 mM Tris, 150 mM NaCl, pH 7.8. Then, ultracentrifugation at 100000*g* for 1 h in a Sorvall Discovery 90 at 4 °C was taken to pellet down any aggregation. The concentration of TnT−Tm was determined from a molar extinction coefficient $\epsilon_{280\ nm}$ of 27 840 M^{-1} cm^{-1}, which is the sum of the molar extinction coefficients from one TnT and two Tm chains.

TnT N47

SDT**E**E**V**E**H**G**E**A**H**E**A**E**E**V HE**E**A**H HE**E**A**H HA**E**A**H HE**E**A**H AHA**E**E**V**H**E**P

TnT 8e16

SDT**E**E**V**E**H**G**E**A**H**E**A**E**E**V HE**E**A**H HE**E**A**H HE**E**A**H HE**E**A**H HA**E**A**H HA**E**A**H HE**E**A**H AHA**E**E**V**H**E**P*APPP* EEKPRIKLTAPKIPEGEKVDFDDIQKKRQNK DLIELQALIDSHFEARRKEEEELVALKERIEKRRAERAEQQRIRAEKEKER QARLAEEKARREEEDAKRKAEDDLKKKKALSSMGASYSSYLAKADQK RGKKQTARETKKKVLAERRKPLNIDHLNEDKLRDKAKELWDWLYQLQ TEKYDFAEQIKRKKYEILTLRCRLQELSKFSKKAGAKGKVGGRWK

FIGURE 1: Sequence of TnT N47 and chicken breast muscle TnT 8e16. TnT N47 is the N-terminal 46-amino acid fragment of chicken breast muscle TnT-1 isoform excluding the first methionine and containing 17 glutamates (as shown in bold) and four of the metal-binding Tx motifs (as marked with boxes). TnT 8e16 is the major isoform of adult chicken breast muscle TnT, which contains 22 glutamates in the N-terminal 61 residues, and seven Tx motifs. A sequence of APPP shown in italic forms the epitope of mAb 3E4 used in Western blot verification of the TnT proteins. The Tx motifs have been proven to have metal ion binding ability, while the polyglutamate composition suggests potential Ca^{2+} binding sites.

Terbium-Binding Assays of TnT. Terbium was used as a calcium analogue to probe the nature of TnT's interaction with calcium due to terbium's more readily detectable fluorescence and high affinity for calcium-binding sites. For these assays, TnT N47 was in 15 mM Tris, 150 mM NaCl, pH 7.8 buffer, and the intact TnT was in the same buffer with an additional 10 mM imidazole to partially quench the unbound Tb^{3+} luminescence. The titration of TnT's with Tb^{3+} were completed by adding aliquots of a freshly prepared Tb^{3+} stock solution to the TnT solution (1 μM), and then Tb^{3+} fluorescence was measured on a SLM Aminco-Bowman II luminescence spectrometer with an excitation wavelength at 248 nm and band-pass at 16 nm. All measurements were performed at room temperature. Tb^{3+}-binding curves were plotted with MacCurve Fit (Kevin Raner Software) and fitted to the following form of the Hill equation:

$$I = I_{max}\, T^n/(K_d + T^n) \qquad (1)$$

in which I is absolute difference in fluorescent intensity, K_d is the apparent dissociation constant of TnT with Tb^{3+}, I_{max} is the maximum absolute difference in fluorescent intensity,

Table 1: Summary of Metal Binding of Three Different Forms of TnT

	Tb^{3+} binding constants			Ca^{2+} binding EC50	
form of TnT	apparent K_d (μM)	n	R^2	EC50 (μM)	R^2
TnT N47	10 ± 3	1.5 ± 0.3	0.96	14.7 ± 6.0	0.80
TnT	5.6 ± 0.8	0.8 ± 0.2	0.98	23.0 ± 8.9	0.80
TnT−Tm	31 ± 4	1 (fixed)	0.99	35.9 ± 11.6	0.79

n is the Hill coefficient, and T is terbium concentration. The results are summarized in Table 1.

Competitive Binding Assays of Tb^{3+} and Ca^{2+}. In this assay, 1 μM TnT N47 or TnT−Tm was incubated with 5 μM Tb^{3+}, followed by titration with high concentration of Ca^{2+}. Time-resolved Tb^{3+} fluorescence excitation spectra were measured in the same way as in Tb^{3+}-binding assays. TnT N47 was in 15 mM Tris, 150 mM NaCl, pH 7.8 buffer, while an additional 10 mM imidazole was added to buffer TnT−Tm complex as Tb^{3+} quencher. The control experiment of Ca^{2+} titration to Tb^{3+} without TnT confirmed that the Ca^{2+} solution has no effect on the Tb^{3+} fluorescence spectra. All measurements were performed at room temperature.

Calcium-Binding Assays of TnT. The Ca^{2+}-binding was measured by a filtration method with $^{45}CaCl_2$ (Amersham Pharmacia) in 15 mM Tris, 150 mM NaCl, pH 7.8 buffer at room temperature. In some experiments, 2 mM $MgCl_2$ was added to the solution to examine if there might be competition between Ca^{2+} and Mg^{2+}. The TnT N47 and TnT−Tm concentrations used for the measurement were 1 μM, and TnT concentration was 2 μM. The concentrations of Ca^{2+} were from 0.5 to 100 μM. The $^{45}CaCl_2$ was added to TnT, and the assay solution was passed through a protein binding membrane on which TnT and its bound Ca^{2+} remained, while free Ca^{2+} flowed through. For TnT N47, the Spartan-3 syringe filter with nylon membrane (Aldrich) was used, whereas mixed cellulose ester membranes (Advantec MFS, Inc.) with a plastic swinney filter holder (PALL Gelman Laboratory) were used for TnT and TnT−Tm Ca^{2+}-binding experiments. The ^{45}Ca radioactivity of the assay solution and its filtrate in identical volumes were measured in a Beckman LS 5000TD liquid scintillation counter, and calibrated to determine the concentrations of total and free Ca^{2+}, respectively. Nonspecific Ca^{2+}-binding to the membrane were corrected. Bound Ca^{2+} was calculated from the difference between total and free Ca^{2+}. In some experiments, the $^{45}Ca^{2+}$ radioactivity of the filter membrane was also measured to directly determine the concentration of bound Ca^{2+}. The experiments were repeated several times. Bound Ca^{2+} was plotted as the function of total Ca^{2+}, and applied to the linear fitting with MacCurve Fit. The EC50 of Ca^{2+}-binding was determined from the linear fitting with Statistica software as the free Ca^{2+} concentration at which the bound Ca^{2+} concentration equals half the TnT concentration. The results are summarized in Table 1.

Calibration of Free Calcium Concentration. Ca^{2+} solutions (4−9 mM) were buffered with 10 mM HEDTA, at pH 7.8, ionic strength 165 mM. The free Ca^{2+} concentrations (1.05−13.2 μM, correspondingly) were calculated from the software MaxC (version 2.40, http://www.stanford.edu/~cpatton/maxc.html). To trace the Ca^{2+} concentration change upon protein binding, calcium green 5N (Molecular Probes), a calcium-sensitive dye that emits high fluorescence when it binds to Ca^{2+} with low background by itself, was mixed with the sample. After its addition to the Ca^{2+} solution, calcium green 5N was excited at 488 nm and band-pass at 16 nm, and its fluorescence was detected by the luminescence spectrometer at 532 nm and band-pass at 4 nm. The standard curve was plotted as fluorescent intensity vs free Ca^{2+} concentration and fitted to a derived function.

$$\text{suppose } C + D \Leftrightarrow B$$

in which C, D, and B stands for free Ca^{2+}, free calcium green 5N, and bound Ca^{2+}, respectively. Then it follows at equilibrium

$$K_d = CD/B \tag{2}$$

Since $D = D_T - B$, in which D_T is the total concentration of calcium green 5N. Equation 2 can be modified as $K_d = C(D_T - B)/B$, and converted to

$$B = D_T/(K_d/C + 1) \tag{3}$$

On the other hand, the measured fluorescent intensity (I) is contributed from both forms of free (I_0) and Ca^{2+} bound (I_{Ca}) calcium green 5N. Moreover, the fluorescent intensity of calcium green 5N is proportional to its concentration, and can be expressed as $I_0 = D/c$, and $I_{Ca} = B/k$. As a result, the fluorescent intensity is

$$I = (D_T - B)/c + B/k \tag{4}$$

Combining eqs 3 and 4, the fluorescent intensity can be expressed as a function of free Ca^{2+} (C) and other constants including K_d (23.0 ± 0.6 μM)

$$I = D_T(1/k - 1/c)/(K_d/C + 1) + D_T/c \tag{5}$$

The constant k (0.031) and c (0.954) were measured by mixing calcium green 5N with 50 mM of Ca^{2+} and EGTA, respectively, and included in eq 5 during curve fitting.

Kinetics Study of TnT−Tm Complex Calcium Binding. Kinetic measurements of TnT−Tm Ca^{2+}-binding were performed with a stopped flow reactor (Milliflow, SLM Aminco) connected with the luminescence spectrometer. The measurements were made in 15 mM Tris, and 150 mM NaCl, 2 mM $MgCl_2$ pH 7.8 at room temperature. TnT−Tm solution (0.3 μM) was mixed rapidly with Ca^{2+} plus calcium green 5N in the stopped-flow reactor driven under a compressed nitrogen pressure of 60 psi. The excitation monochromator was set to 488 nm (band-pass 16 nm), and the fluorescence emission of calcium green 5N was monitored at 532 nm (band-pass 4 nm). Reaction curves were obtained by averaging at least 60 reaction traces. Data were plotted and fitted with the MacCurve Fit software. The reaction traces were analyzed for the first 200 ms for fast binding rate constants. Since the time constant for calcium dissociation from calcium green 5N is less than 1 ms, and the data were collected at 1 ms resolution (*24*), the fluorescent intensity was taken as faithful indicator of free calcium levels. Control mixing experiments at fixed free calcium levels demonstrated that the dye fluorescence was not affected by the presence of the proteins used.

To process the reaction trace data for rate constants fitting, a kinetics equation was derived below:

$$\text{suppose } P + C \underset{k_{off}}{\overset{k_{on}}{\leftrightarrows}} B$$

in which *P*, *C*, and *B* stands for calcium-binding sites on the protein, free Ca^{2+}, and bound Ca^{2+}, respectively. Then, it follows

$$dC/dt = -k_{on}PC + k_{off}B \quad (6)$$

The concentrations of total, free, and bound protein or Ca^{2+} are constrained by

$$P = P_T - B \quad B = C_T - C \quad (7)$$

Taking eqs 6 and 7 together, the change of free Ca^{2+} concentration per time (dC/dt) can be expressed in terms of free Ca^{2+} concentration (C) in eq 8

$$dC/dt = -k_{on}C^2 + (k_{on}C_T - k_{on}P_T - k_{off})C + k_{off}C_T \quad (8)$$

where k_{on} is the Ca^{2+}-binding rate constant, k_{off} is Ca^{2+} dissociation rate constant, C_T is concentration of total Ca^{2+}, and P_T is concentration of calcium-binding sites on the protein.

Equation 8 was taken further two consecutive derivatives with respect to free calcium concentration (C) to eliminate all other parameters and constants except k_{on}.

$$\frac{\partial^2(dC/dt)}{\partial C^2} = -2k_{on} \quad (9)$$

The intensity from reaction traces was calibrated into concentration of free Ca^{2+}. The change of free Ca^{2+} per millisecond was taken as the first derivative with respect to time and two additional derivatives with respect to free Ca^{2+} were determined graphically as indicated in eqs 8 and 9. The Ca^{2+}-binding on-rate and its 95% confidence limits were calculated from the averaged third derivative data.

Molecular Mechanics Simulations of TnT N47. Computations were performed using Macromodel (version 8.1, Schrödinger, Inc.) and an OPLS-AA or a MMFF (used for Zn^{2+} binding simulations only, since it has been parametrized for handling transition metals with a commonly used nonbonded model) second generation all atom force fields on a 2 GHz LINUX workstation with 2 gigabytes RAM. Unless otherwise specified, a GB/SA (generalized Born/solvation area) solvent model was employed, and only high quality parameters were used for the structure prediction calculations with the OPLS-AA force field as described (*25*).

The structure of the peptide TnT N47 was predicted de novo from free energy calculations using a combination of energy minimizations, low-frequency mode searches, Monte Carlo conformational searches, and stochastic dynamics simulations. First, the sequence of TnT N47 was build in an α-helical conformation, since the amino acid composition has a high predicted propensity for this secondary structure and previous circular dichroism studies suggested that this secondary structure was partially present (*15*). Energy minimizations with harmonic distance constraints were used to steer the valine residues (the only strongly hydrophobic residues in the peptide) into close proximity with each other to build a hydrophobic core. Then, the distance constraints were eliminated, and the structure entered a stochastic dynamics simulation for 1 ns using 1.5 fs steps with SHAKE algorithms for all bonds. Next, a mixed low frequency mode and Monte Carlo conformational search yielded 92 unique lowest energy structures within 50 kJ/mol of the apparent global minimum, and 45 duplicate structures were also found. Cluster analysis indicated that 89 of the 92 unique structures had a nearly identical fold with less than 0.35 nm RMSD of their heavy atoms. This class of structures comprised 84 out of the 84 the structures within 26 kJ/mol of the apparent global minimum, so a large proportion of the identified lowest energy structures were closely matched in structure and energy level which is consistent with a stable folded conformation. Seeded repeats of this conformational search produced similar results. A more detailed description of the algorithm and validation studies are included in Supporting Information. A simulated annealing approach based on a published protocol (*26*) that has been successful on smaller peptides was tried for comparison to the rationally directed approach described above; however, it generated random coils with higher energy than the stable folded conformation predicted above.

A calcium ion binding pocket was identified using a 2 ns stochastic dynamics simulation on the lowest energy structure in the presence of a calcium ion. To accelerate interaction between the metal ion and the protein on this time scale, a distance-dependent dielectric model was used in place of GB/SA water model (*27*−*28*). The resulting structure was then minimized to convergence and analyzed with two different 100 ps molecular dynamics simulations using the GB/SA water model and also explicit solvent with periodic boundary conditions and particle mesh Ewald electrostatics (using TINKER 4.0; *29*). During both simulations, the calcium ion remained bound within the internal pocket, and structures demonstrated typical coordination of the calcium by eight oxygen atoms. Further stochastic dynamics simulations using the distance-dependent dielectric solvent model revealed the effects of multiple calcium or zinc ions on the TnT N47 conformation.

RESULTS

Three forms of TnT were used for binding studies, TnT N47, TnT, and TnT−Tm. The TnT N47 is an N-terminal fragment to verify that the binding occurs at this N-terminal region (see Figure 1). Highly purified TnT was used to demonstrate binding to the intact protein. Tm interacts with TnT including one binding site in the N-terminal T1 region (*30*), and likely has effects on the conformation of TnT. Therefore, the TnT−Tm complex was prepared for some of the Ca^{2+}-binding experiments. Overloaded samples in Figure 2 not only prove greater than 97% purity of the TnT and Tm preparations as quantified by gel densitometry, but also provide evidence that potential contaminating calcium-binding proteins such as TnC and parvalbumin, which have much lower molecular weights than TnT and Tm, have been eliminated.

The SDS−PAGE gel in Figure 2 also shows that the molar ratio is consistent with one TnT to one Tm dimer.

Binding of Terbium to TnT. Tb^{3+} is a lanthanide analogue of calcium often used to probe the nature of protein interactions with Ca^{2+} (*31*−*33*). Tb^{3+} has a similar ionic radius to that of Ca^{2+} in aqueous solution, and has the

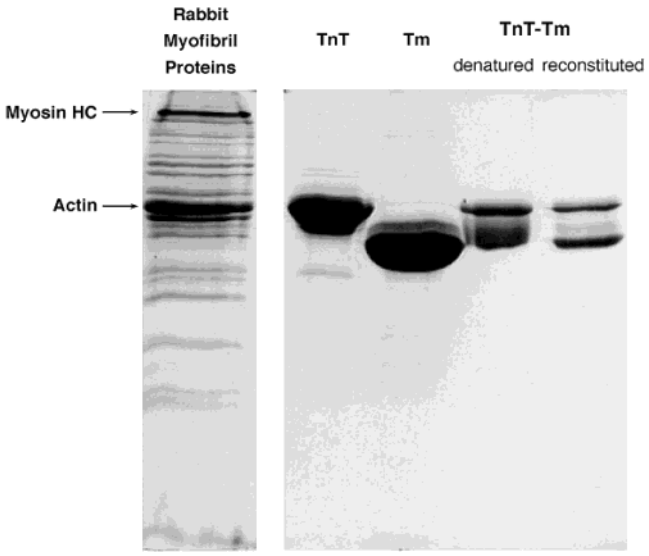

FIGURE 2: Purity and reconstitution of proteins assayed. Protein fractions from chromatography or dialysis were examined by 15% SDS−PAGE, and the gel picture was captured from a CCD camera. Preparation of TnT−Tm complex. SDS−PAGE shows the process of renaturing. Samples applied to each lane were as follows: rabbit skeletal muscle proteins, chicken breast muscle TnT, rabbit skeletal muscle Tm, denatured TnT and Tm mixture, and reconstituted TnT−Tm complex after renaturing. Protein purity was estimated from video densitometry as greater than 97% in all cases.

advantage of easily detectable fluorescence. Because of the increased charge of Tb^{3+} compared with Ca^{2+}, Tb^{3+} sometimes has a higher affinity for Ca^{2+}-binding sites than does Ca^{2+} itself. In the Tb^{3+} titration measurements of TnT, TnT N47, and TnT−Tm complex, significant fluorescence changes have been measured, demonstrating that they bind to Tb^{3+} with high affinity (10^5-10^6 M^{-1}). Figure 3A shows the decrease of Tb^{3+} fluorescence upon its binding to TnT N47. From the fluorescent change, a TnT N47 Tb^{3+}-binding curve was plotted (Figure 3B), and an apparent dissociation constant of TnT N47 to Tb^{3+} obtained from curve fitting is in low micromolar range (10 ± 3 μM).

In the measurement of chicken breast muscle TnT and TnT−Tm Tb^{3+}-binding, 10 mM imidazole was added to buffer and acted as a quencher. As a result, Tb^{3+} by itself showed weak fluorescence, while exhibiting more than a 2-fold increase in fluorescence with a slight red-shift of the peak after adding TnT−Tm (Figure 3C,E). The binding curves of TnT 8e16 and TnT−Tm with Tb^{3+} are plotted in Figure 3, panels D and F, respectively.

The apparent K_d values of the different forms of TnT's binding to Tb^{3+} are summarized in Table 1. The very similar Tb^{3+}-binding affinity of TnT N47 and intact chicken breast muscle TnT demonstrates that Tb^{3+} binds to the N-terminal region of TnT. However, TnT−Tm complex exhibits slightly lower affinity to Tb^{3+} than TnT N47 and free breast muscle TnT. This decreased affinity to Tb^{3+} might be a result of Tm altering the N-terminal conformation of TnT. A mild degree of positive cooperativity was detected in TnT N47 ($n = 1.5 \pm 0.3$), but was not apparent in the intact TnT. The data for TnT−Tm did not yield a unique value for the Hill coefficient, so a value of $n = 1$ was used to estimate the apparent K_d (Table 1).

Competitive Binding of Ca^{2+} with Tb^{3+} to TnT. To verify that Ca^{2+} and Tb^{3+} bind to similar sites on TnT, competitive assays were performed. Figure 4 demonstrates that for both TnT N47 (Figure 4A) and TnT−Tm (Figure 4B) the added Ca^{2+} is able to displace prebound Tb^{3+}. This control indicates that at least some of the ion binding sites can be bound by either Ca^{2+} or Tb^{3+}. However, a given site might have a stronger affinity for one of the two ions.

Binding of Calcium to TnT. Avian adult breast muscle TnT has been classified as acidic TnT because of the polygultamates in its N-terminal region. In contrast, avian leg muscle TnT's are basic isoforms. The glutamate-rich sequence is proposed to possess Ca^{2+}-binding ability in the chicken breast muscle TnT.

To determine the binding of Ca^{2+} to TnT, radioactive ^{45}Ca was applied with the filtration method. The results of Ca^{2+}-binding measurements are shown in Figure 5, and the EC50's obtained are summarized in Table 1. The binding data showed that the minimum number of calcium ions binding to TnT N47 is approximately two per molecule (Figure 5A); however, that of the intact TnT and TnT−Tm appears to be one per molecule (Figure 5B,C). The possible reason could be that TnT N47 is more flexible than intact TnT and TnT−Tm so that it binds to more Ca^{2+}. Although the fitting did not result in precise K_d values, the EC50 is clearly in the micromolar range, which is close to the Ca^{2+} activation concentration in muscle fibers. Ca^{2+}-binding activity of TnT−Tm was also examined in the presence of 2 mM $MgCl_2$. The binding isotherm was not altered (data not shown), indicating that Mg^{2+} is not competitive with the Ca^{2+}-binding sites on TnT.

TnT−Tm Calcium-Binding Rate. The stopped-flow experiments were performed to study the kinetics of Ca^{2+} binding to TnT−Tm. A solution containing TnT−Tm was mixed with a solution of Ca^{2+} plus calcium green 5N, and the Ca^{2+} binding was observed by following the fluorescence intensity change of calcium green 5N. The resultant stopped-flow trace is shown in Figure 6. Fluorescent intensity of calcium green 5N decreased quickly after Ca^{2+} was mixed with TnT−Tm, and significantly up to 5 s. Decreased fluorescence implies Ca^{2+} released from calcium green 5N, and bound to TnT−Tm. The same experiment repeated with Tm only showed no fluorescence change at all. This experiment clearly demonstrated that TnT−Tm has the ability to bind Ca^{2+}. The trace in Figure 6 was more consistent with a double exponential decay ($R^2 = 0.99$) than a single-exponential decay ($R^2 = 0.97$). This fitting indicates that TnT exhibits at least two classes of Ca^{2+}-binding sites. Fast binding happened within 200 ms, and slow binding took place after 200 ms. The slow binding phase is too slow to affect a muscle twitch, so only the fast binding phase was processed for rate constants calculation. The binding rate calculated from the third derivative analysis is $4 \times 10^6 \pm 3 \times 10^6$ M^{-1} s^{-1}, which is significant compared to the speed of the Ca^{2+} transient during the muscle twitch.

Molecular Mechanics Predictions of the Calcium Binding Structure. Computational simulations using molecular mechanics on the TnT N47 peptide were considered to be feasible due to the small size of this peptide. The peptide structure prediction algorithm is related to several recent methods that successfully predict the structures of small single domain proteins with resolutions typically better than 0.7 nm RMSD (*26*, *29*, *34*−*36*). In contrast to secondary structure predictions based on its amino acid composition,

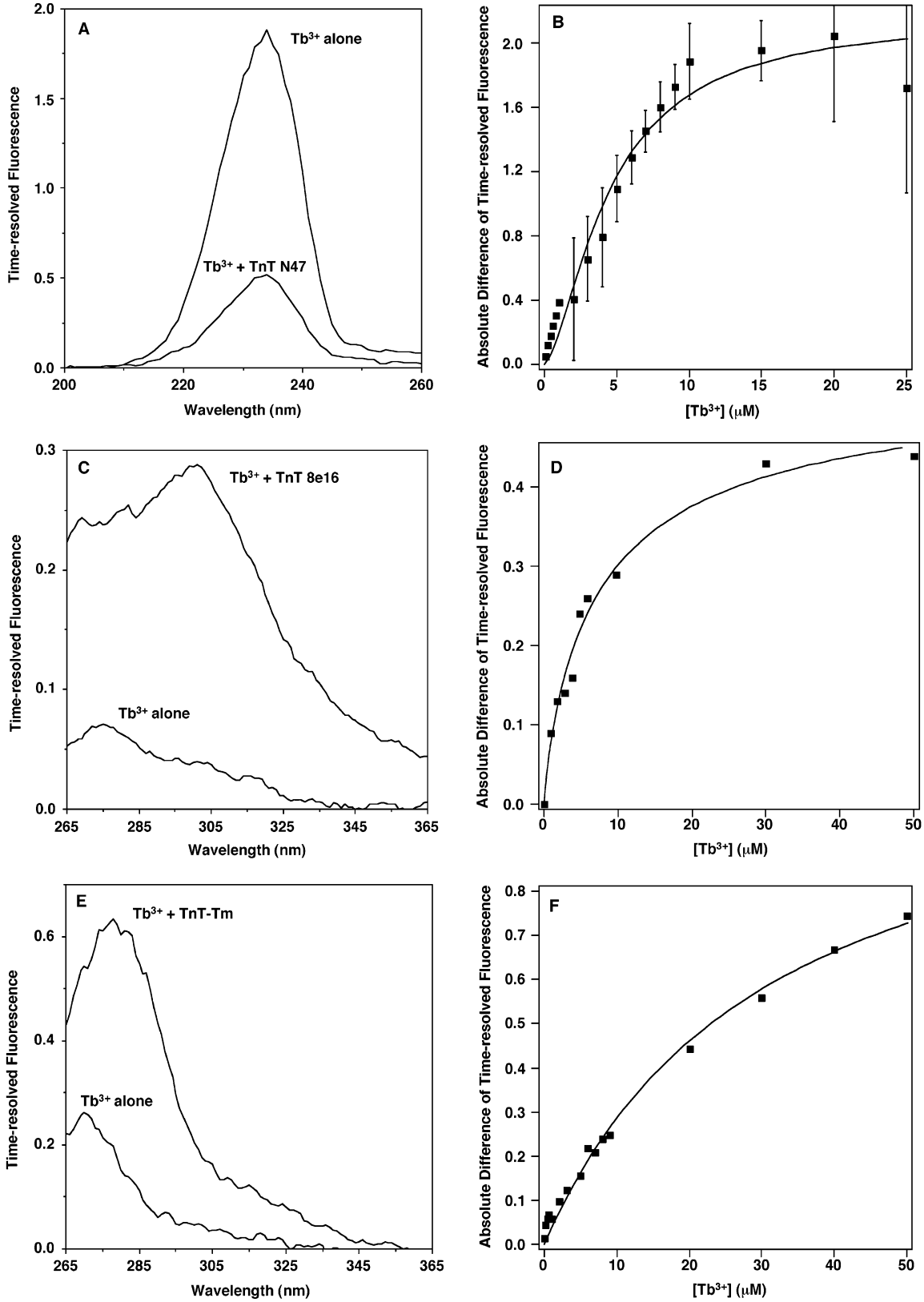

FIGURE 3: Tb^{3+} binding to TnT and its N-terminal fragment, N47. The time-resolved fluorescent excitation spectra of Tb^{3+} (4.8 μM) were measured upon its binding to 1 μM TnT N47 (A), TnT 8e16 (C), and reconstituted TnT−Tm (E). Compared to Tb^{3+} alone, a significant decrease of fluorescent intensity at 234 nm was observed upon the binding to TnT N47 (A), while the increased fluorescence with peak shifts in 265 to 365 nm were measured when Tb^{3+} binds to TnT 8e16 (C) and TnT−Tm (E). The time-resolved fluorescence intensities were measured at 547 nm for 0.2−4.5 ms after a 0.001 ms excitation pulse at the wavelength given on the horizontal axis. The changes of fluorescent intensity were processed to plot the Tb^{3+} binding curve for 1 μM TnT N47 (B), 1 μM TnT 8e16 (D), and 1 μM TnT−Tm (F). Nonlinear curve fitting of the binding curves with the Hill equation yielded Tb^{3+} binding constants as summarized in Table 1. Error bars show the representative standard deviations. The calculated apparent K_d values are reported in Table 1.

the free energy calculations indicate that this peptide is more than just an α-helix, since the alternative folded conformations yield more stable lower energy structures. Although the peptide is too large to permit exhaustive conformational

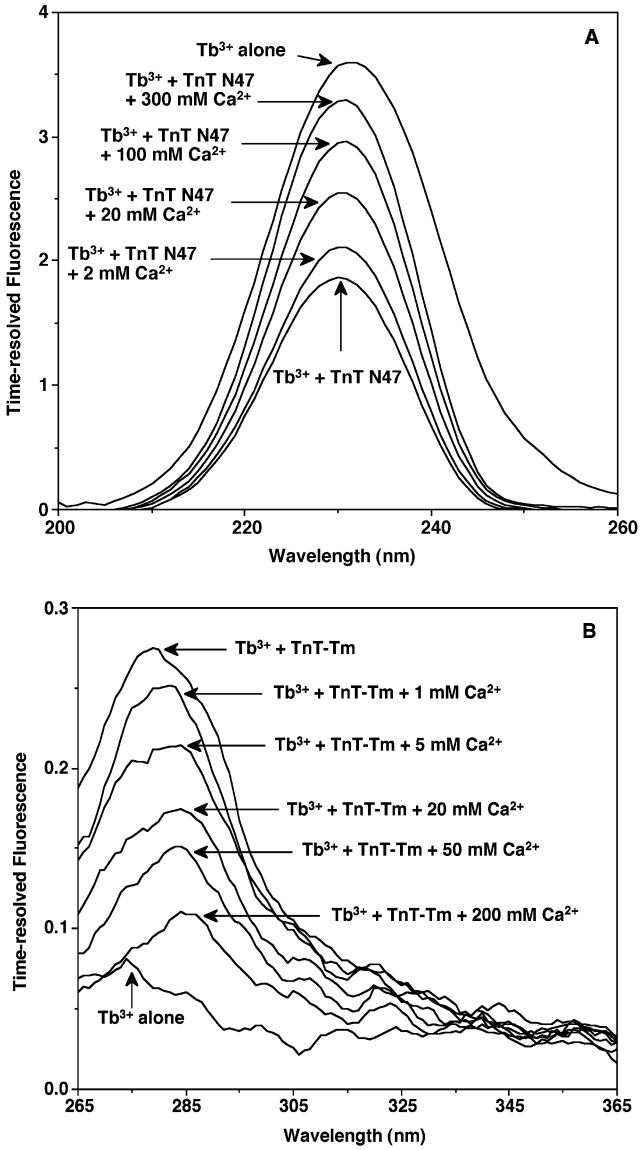

FIGURE 4: Ca^{2+} competitive binding of Tb^{3+} to 1.0 μM TnT N47 (A) and reconstituted TnT−Tm complex (B). The time-resolved fluorescent excitation spectra of Tb^{3+} (5 μM) were measured as signal that Tb^{3+} binds to TnT or not. Compared to Tb^{3+} alone, the decreased fluorescence of Tb^{3+} at 230 nm was resumed back to the level of Tb^{3+} alone. In the assay using TnT−Tm, the increased fluorescence with peak shifts in 265 to 365 nm were dropped after adding Ca^{2+}.

searches, the results of the mixed low energy mode and Monte Carlo conformational searches were promising because they converged to a single class of lowest energy structures. While this structure might still be considered speculative, it is consistent with previous circular dichroism measurements on this peptide (*15*) which estimated approximately 4−10% α-helix, 1−11% β-sheet, 21−47% β-turns, and 46−64% other structures. By comparison, the lowest energy de novo predicted structure contains one short α-helix (9%), one short three-stranded antiparallel β-sheet (9%), eight turns (46%; 17% β-turns), and a substantial amount of intervening structures (37%). Furthermore, the calculated interaction energy using the apparent global minima of TNT N47 with a single Ca^{2+} was in close agreement with the experimental binding free energy, −6 versus −7 kcal/mol, respectively (*37*−*39*, see Supporting Information for details).

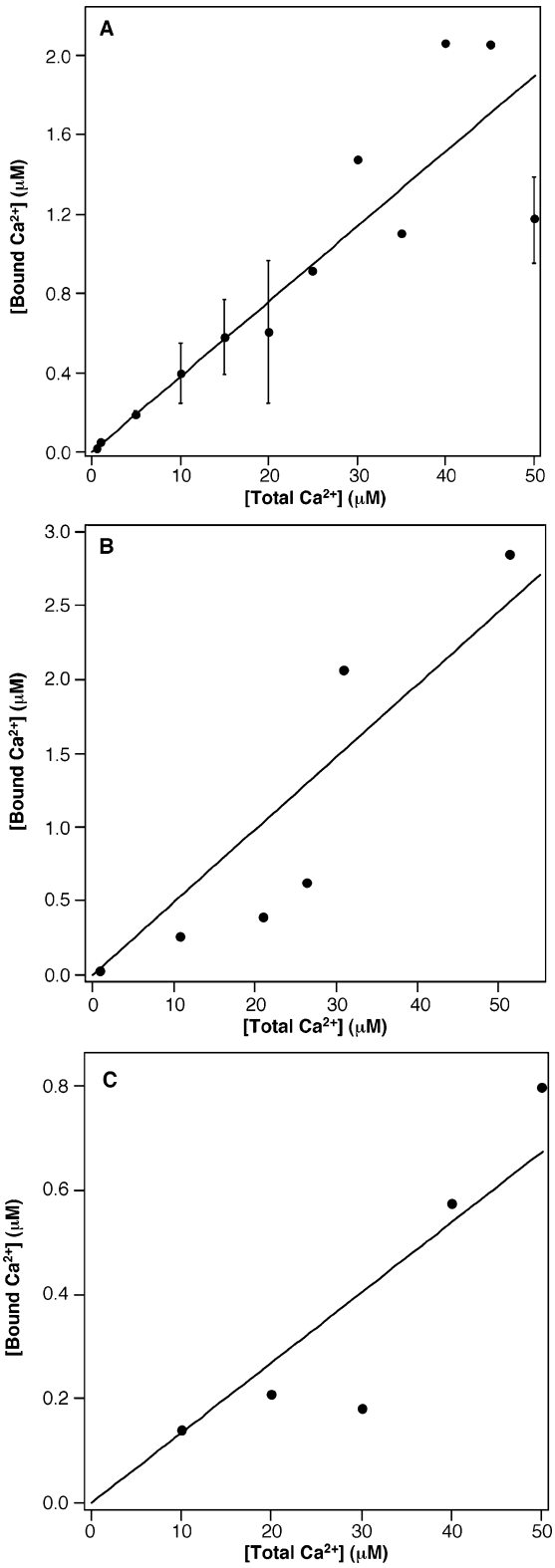

FIGURE 5: Linear fitting of Ca^{2+} binding curves of 1 μM TnT N47 (A), 2 μM TnT (B), and 1 μM TnT−Tm (C). The lack of apparent saturation indicates that multiple classes of sites with different affinities for $^{45}Ca^{2+}$ are present. The $^{45}Ca^{2+}$ binding to TnT's were carried out by filtration as described in methods. The concentration of bound Ca^{2+} is plotted versus that of free Ca^{2+}. Error bars in A and C stand for standard deviation from three and five measurements, respectively. In A and B, bound Ca^{2+} concentrations were calculated from the differences between concentrations of total and free Ca^{2+}, while in C, it was directly calibrated from the radioactivity of the cellulose membrane. The calculated EC50 values are summarized in Table 1.

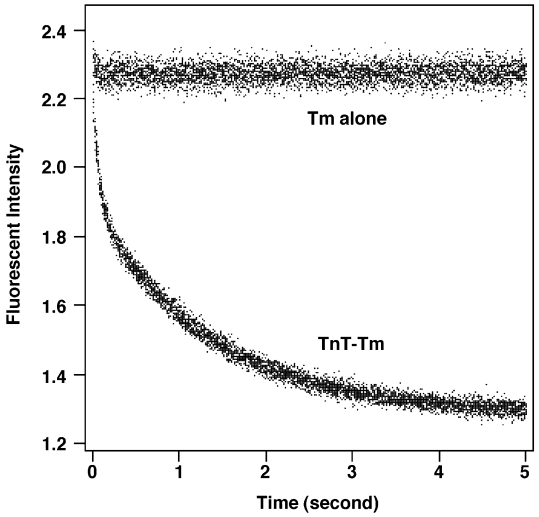

FIGURE 6: Stopped-flow trace for the Ca^{2+} binding of TnT−Tm complex. TnT−Tm solution was mixed rapidly with calcium plus calcium green 5N in the stopped flow reactor, and the time-course of Ca green 5N fluorescent intensity change was observed in 1 ms intervals by the luminescence spectrometer. The decrease of intensity indicates dissociation of calcium from the calcium dye due to calcium binding to TnT−Tm. The apparent double exponential decay implies that at least two binding components with different affinities exist in TnT. In contrast, the control experiment on top with Tm alone showed no change of fluorescent intensity indicating no calcium ion binding to Tm.

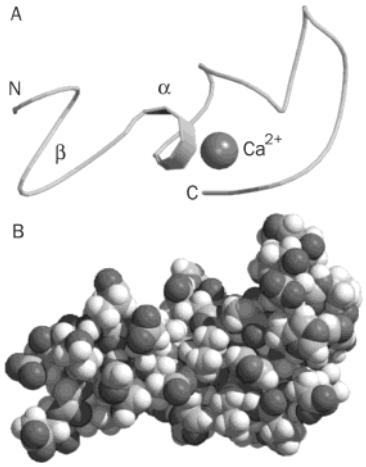

FIGURE 7: Schematic and space filling structures of TnT N47 upon one Ca^{2+} binding. The predicted atomic model of TnT N47 following a 2 ns stochastic dynamics simulation with a single Ca^{2+} and subsequent energy minimization for 200 steps with an OPLS-AA force field and GB/SA solvent model. The schematic representation (A) shown above and the space filling model (B) below illustrate the same structure and orientation. The α denotes α-helix, the β denotes β-sheet, the N denotes the N-terminus, and the C denotes the C-terminus in the schematic model. Note the Ca^{2+} is barely visible within its pocket even from the best of viewing angles in the space filling model. The figure was generated with Molscript and Raster 3D software (*46*−*47*).

Stochastic dynamics simulations of the TnT N47 with Ca^{2+} suggest a plausible mechanism for Ca^{2+} binding. During the course of the simulation, the Ca^{2+} enters a pocket on the TnT N47 in the Tx motif region. Then, the C-terminal end of the peptide seals the Ca^{2+} inside the binding pocket. A combination of carboxylic acids and peptide backbone carbonyls coordinate with the Ca^{2+} to stabilize its position. The overall fold of the peptide changes modestly during the simulation. The RMSD between the initial peptide conformation and the final peptide conformation during the simulation is 0.47 nm. Similar results are obtained in the presence or absence of a methyl amide group attached to C-terminus to simulate a peptide bond indicating that a similar fold might occur in the intact version of the TnT protein. Interestingly, the Ca^{2+}-binding pocket is comprised primarily of the short α-helix and a loop which is reminiscent of the EF hand Ca^{2+}-binding structure. The electrostatic interactions between the positively charged histidines and the negatively charged glutamates of the Tx motif stabilize this loop fold near the helix to form the Ca^{2+}-binding pocket. We suspect that similar folding principles may apply to longer repeats of the Tx motif in TnT isoforms that may contain additional Ca^{2+}-binding pockets.

DISCUSSION

TnT is one of the major regulatory proteins in striated muscle, which interacts with TnC, TnI, and Tm during muscle contraction. TnT has diverged into multiple isoforms in different muscle tissues. Adult avian breast muscle TnT differs from the leg muscle TnT in the presence of a cluster of metal binding motifs in the N-terminal region. Ca^{2+} sensitivity in different chicken muscles differs according to their TnT isoform contents (*19*). While it is well established that Ca^{2+} binding to the TnC triggers the contraction of striated muscle, the present study demonstrates that at least some TnT isoforms bind Ca^{2+} with potentially competitive affinities and rate constants. In our study, Ca^{2+} binding to chicken breast muscle TnT was measured directly using radioactive and fluorescent probes. Chicken breast muscle TnT binds to Ca^{2+} as well as Tb^{3+} with high affinity (10^5−10^6 M^{-1}). The binding occurs in the N-terminal region of the TnT molecule, because TnT N47 exhibits similar Ca^{2+}- and Tb^{3+}-binding properties to the intact TnT. The Ca^{2+}-binding sites are proposed to be in the glutamate-rich segment. In addition, the chicken breast muscle TnT binds to Ca^{2+} with an on-rate of 4×10^6 M^{-1} s^{-1}. Although this on-rate is somewhat slower than that reported for TnC, it is quick enough to impact the striated muscle twitch cycle.

Calcium Binding to TnT. To measure the affinity of Ca^{2+} to different forms of chicken breast muscle TnT, radioactive $^{45}Ca^{2+}$ was used in membrane filtration experiments. High signal-to-noise ratio $^{45}Ca^{2+}$ radioactivity successfully proved that adult chicken breast muscle TnT has affinity to Ca^{2+} in low micromolar range and is consistent with multiple calcium ions binding per protein molecule (Figure 5). This Ca^{2+}-binding affinity is similar to the physiological Ca^{2+} trigger sites in the N-domain of TnC which has an affinity of $\sim 10^5$ M^{-1} and is highly selective of Ca^{2+} over Mg^{2+} (*40*). Moreover, the Ca^{2+}-binding curves in Figure 5 seem not to be reaching the plateau or in other words, TnT was not saturated with Ca^{2+}. It is likely that TnT has multiple Ca^{2+}-binding sites but with different affinities to Ca^{2+}. In contrast, the terbium binding data demonstrated clear hyperbolic binding isotherms that probably reflect only the highest affinity metal ion binding site that influences the fluorescent properties. The predicted atomic model of TnT N47 is consistent with this interpretation, since only the highest affinity Ca^{2+}-binding site is well sheltered from the solvent (Figure 7).

Table 2: RMSD Comparisons of Dynamic Atomic Models with Metal Ions

condition[a]	0 OPLS	1 Ca^{2+}	10 Ca^{2+}	0 MMFF	1 Zn^{2+}	10 Zn^{2+}
0 OPLS	0	0.47 nm	0.60 nm	0.44 nm	0.77 nm	0.90 nm
1 Ca^{2+}	x	0	0.41 nm	0.43 nm	0.51 nm	0.67 nm
10 Ca^{2+}	x	x	0	0.62 nm	0.68 nm	0.56 nm
0 MMFF	x	x	x	0	0.53 nm	0.91 nm
1 Zn^{2+}	x	x	x	x	0	0.98 nm

[a] The OPLS-AA force field was used for Ca^{2+} simulations and MMFF was used for Zn^{2+} simulations, since MMFF contains parameters for transition metal ions. The number of metal ions used in a 2 ns stochastic dynamics simulation is given.

Toward an Atomic Model of Metal Ion Binding to TnT. The predicted atomic model in Figure 7 is consistent with several experimental observations on TnT N47. The relative amounts of secondary structure match those measured by circular dichroism (*15*). The sheltered nature of the high affinity metal ion binding site is consistent with the detection of changes in Tb^{3+} fluorescence upon binding. Its elongated form concurs with the expected structure of TnT based on its sedimentation coefficient (*17*). The calculated and experimental ion binding energies are consistent.

Considering this excellent agreement, the atomic model was evaluated in simulations with varying numbers of calcium and zinc ions. While both calcium and zinc ions could bind within the high affinity metal ion binding pocket of the TnT N47 atomic model, calcium formed more extensive coordinations with the amino acid residues. Similarly, when as many as 10 metal ions were included during dynamics simulations, only one bound in a tight pocket while the others associated more loosely with external amino acids. As many as six of the 10 calcium ions had significant interaction energies with TnT N47 in the simulations. The structural effects of the binding of these metal ions on the TnT N47 atomic model are summarized in Table 2. The binding of multiple zinc ions caused the most substantial structural changes in the TnT N47 with an RMSD of nearly a nanometer in the C_α carbons. The binding of calcium ion had comparatively little effect on the conformation, since the differences between OPLS-AA and MMFF force fields (RMSD = 0.44 nm) suggested nearly as much conformational fluctuation as the calcium binding induced structural change (RMSD = 0.47 nm). The effect of transition metal ion binding on TnT structure is highly consistent with previous spectroscopic measurements (*15*, *17*), while effects of calcium ion binding on TnT structure have not yet been detected experimentally. These experimental data support this atomic model as a starting point for interpreting the interactions of the Tx motifs with calcium ions at the atomic level.

What Are the Possible Physiological Roles of Calcium Ion Binding to TnT? Given the data supporting the binding of calcium ions to TnT isoforms containing the Tx motifs at affinities comparable to the binding of calcium ions to TnC, there are several hypothetical scenarios as to its physiological significance. The binding to metal ions is selective, since calcium and terbium ions bind with higher affinity than zinc or copper ions, and magnesium ions do not compete with the calcium or terbium ions. Among the TnT-binding ions, only Ca^{2+} are present at concentrations that would permit significant binding in muscle cells, the data indicate that calcium should be bound by the Tx motifs during a calcium transient. Troponin is present in the myofibril at a concentration of approximately 10^{-4} M, while the free calcium ion concentration during activation is only about 10^{-6} M, so TnT would not need to be saturated to compete for a significant fraction of the free calcium in the myofibril that is cooperatively activated by calcium ion binding to TnC. The value of this competition might be to increase the rate of relaxation of the myofibril. The measured on-rate for calcium ion binding to TnT−Tm is on the order of 10^6−10^7 M^{-1} s^{-1}, which is slower than the reported values for TnC. It is plausible that the TnT isoform might compete for calcium toward the end of a calcium wave to reduce the twitch length. Introduction of calcium chelators into muscle have been shown to have this effect (*41*). It is not difficult to see the advantage of a faster twitch cycle in avian flight muscles that control the beating of wings.

Interestingly, parvalbumin is absent from chicken breast muscle where the Tx motif is highly expressed (*42*). Given the affinity of chicken parvalbumin for calcium ion of about 10^6 M^{-1} (*42*) and an off-rate of approximately 1 s^{-1} (*43*), the calculated on-rate (roughly 10^6 M^{-1} s^{-1}) for chicken parvalbumin should be similar to the measured value for chicken breast TnT. It has been demonstrated that transfection of parvalbumin cDNA into muscle increases its relaxation rate (*44*). This proposed function for parvalbumin may be similar to that of the Tx region of TnT except the close proximity of the TnT to TnC should amplify the kinetic effect.

Alternative roles of calcium ion binding by TnT are also possible. The calcium and terbium ion binding data indicate that interactions between Tm and TnT modulate the binding affinity of TnT for metal ions. Previous observations found that copper ions can alter the structure of TnT along its entire length (*17*). These data suggest that structural communication via Tm along the length of the thin filament such as in an allosteric switch type model (*45*) might be linked in part to metal ion binding to the Glu rich N-terminal region of TnT. Yet another hypothesis is that the presence of addition calcium ion binding sites within the myofibril might act as a reservoir to help localize more calcium ions within the myofibril and enhance calcium sensitivity. Consistent with this hypothesis, skinned muscle fibers with high amounts of Tx containing TnT isoforms tend to have higher calcium sensitivity than those lacking the Tx segment (*19*).

While the data presented here with highly purified TnT proteins clearly demonstrate the capacity of these isoforms to bind calcium ions with physiologically relevant affinities, it is not yet possible to directly verify that calcium ion binding to TnT occurs in the muscle fiber. The binding of TnT to Tm has been shown to modulate calcium ion binding, so it is conceivable that the other components of the thin filament may impact the calcium ion binding properties of TnT. Further studies are required to evaluate such issues.

In summary, the data indicate that the Tx motifs of adult avian pectoral TnT can bind calcium ions with high affinity, specificity, and fast on-rate constants. To interpret these observations from a structural perspective, a dynamic atomic model was predicted of an N-terminal TnT fragment containing the Tx motif that is consistent with the measured spectroscopic and metal ion binding properties. The calcium-binding properties of TnT isoforms containing this motif support the view that isoforms of TnT generated by alterna-

tive splicing variations in the N-terminal region can impact the thin filament regulation of muscle contraction.

SUPPORTING INFORMATION AVAILABLE

A detailed description of the computational algorithms used in generating the atomic models, including an algorithm for peptide structure prediction, its testing with the villin headpiece protein, a linear response method (LRM) for calcium ion binding free energy estimation, and tests of the LRM on a variety of calcium chelates. In addition, more experimental evidence of the purity and integrity of the proteins used in this study are presented. This material is available free of charge via the Internet at http://pubs.acs.org.

REFERENCES

1. Leavis, P. C., and Gergely, J. (1984) Thin filament proteins and thin filament-linked regulation of vertebrate muscle contraction. *CRC Crit. Rev. Biochem. 16*, 235−305.
2. Tobacman, L. S. (1996) Thin filament-mediated regulation of cardiac contraction. *Annu. Rev. Physiol. 58*, 447−81.
3. Heller, W. T., Abusamhadneh, E., Finley, N., Rosevear, P. R., and Trewhella, J. (2002) The solution structure of a cardiac troponin C-troponin I-troponin T complex shows a somewhat compact troponin C interacting with an extended troponin I-troponin T component. *Biochemistry 41*, 15654−63.
4. Smillie, L. B., Golosinska, K., and Reinach, F. C. (1988) Sequences of complete cDNAs encoding four variants of chicken skeletal muscle troponin T. *J. Biol. Chem. 263*, 18816−20.
5. Breitbart, R. E., and Nadal-Ginard, B. (1986) Complete nucleotide sequence of the fast skeletal troponin T gene. Alternatively spliced exons exhibit unusual interspecies divergence. *J. Mol. Biol. 188*, 313−24.
6. Cooper, T. A., and Ordahl, C. P. (1985) A single cardiac troponin T gene generates embryonic and adult isoforms via developmentally regulated alternate splicing. *J. Biol. Chem. 260*, 11140−8.
7. Jin, J. P., and Lin, J. J. C. (1989) Isolation and characterization of cDNA clones encoding embryonic and adult isoforms of rat cardiac troponin T. *J. Biol. Chem. 264*, 14471−7.
8. Jin, J. P., Huang, Q. Q., Yeh, H. I., and Lin, J. J. C. (1992) Complete nucleotide sequence and structural organization of rat cardiac troponin T gene. A single gene generates embryonic and adult isoforms via developmentally regulated alternative splicing. *J. Mol. Biol. 227*, 1269−76.
9. Jin, J.-P., and Samanez, R. (2001) Evolution of a metal-binding cluster in the NH_2-terminal variable region of avian fast skeletal muscle troponin T: functional divergence on the basis of tolerance to structural drifting. *J. Mol. Evol. 52*, 103−16.
10. Wilkinson, J. M., Moir, A. J. G., and Waterfield, M. D. (1984) The expression of multiple forms of troponin T in chicken fast-skeletal muscle may result from differential splicing of a single gene. *Eur. J. Biochem. 143*, 47−56.
11. Miyazaki, J., Jozaki, M., Nakatani, N., Watanabe, T., Saba, R., Nakada, K., Hirabayashi, T., and Yonemura, I. (1999) The structure of the avian fast skeletal muscle troponin T gene: seven novel tandem-arranged exons in the exon x region. *J. Muscle Res. Cell Motil. 20*, 655−60.
12. Wilkinson, J. M. (1978) The components of troponin from chicken fast skeletal muscle. *Biochem. J. 169*, 229−38.
13. Ogut, O., and Jin, J.-P. (1998) Developmentally regulated, alternative RNA splicing-generated pectoral muscle-specific troponin T isoforms and role of the NH_2-terminal hypervariable region in the tolerance to acidosis. *J. Biol. Chem. 273*, 27858−66.
14. Jin, J.-P., and Smillie, L. B. (1994) An unusual metal-binding cluster found exclusively in the avian breast muscle troponin T of *Galliformes* and *Craciforms*. *FEBS Lett. 341*, 135−40.
15. Ogut, O., and Jin, J.-P. (1996) Expression, Zinc-Affinity purification, and characterization of a novel metal-binding cluster in troponin T: metal-stabilized α-helical structure and effects of the NH2-terminal variable region on the conformation of intact troponin T and its association with tropomyosin. *Biochemistry 35*, 16581−90.
16. Wang, J., and Jin, J.-P. (1998) Conformational Modulation of Troponin T by Configuration of the NH_2-Terminal Variable Region and Functional Effects. *Biochemistry 37*, 14519−28.
17. Jin, J.-P, and Root, D. D. (2000) Modulation of troponin T molecular conformation and flexibility by metal ion binding to the NH_2-terminal variable region. *Biochemistry 39*, 11702−13.
18. Tobacman, L. B. (1988) Structure−function studies of the amino-terminal region of bovine cardiac troponin T. *J. Biol. Chem. 263*, 2668−72.
19. Ogut, O, Granzier, H., and Jin, J.-P. (1999) Acidic and basic troponin T isoforms in mature fast-twitch skeletal muscle and effect on contractility, *Am. J. Physiol.: Cell Physiol. 276*, C1162−70.
20. Aitken, A., and Learmonth, M. P. (2002) Protein determination by UV absorption in *The Protein Protocols Handbook* (Walker, J. M., Ed.) 2nd ed., pp 3−6, Humana Press, New Jersey.
21. Smillie, L. B. (1982) Preparation and identification of α- and β-tropomyosins. *Methods Enzymol. 85*, 234−41.
22. Luo, Y., Wu, J.-L., Li, B., Langsetmo, K., Gergely, J., and Tao, T. (2000) Photo-cross-linking of benzophenone-labeled single cysteine troponin I mutants to other thin filament proteins. *J. Mol. Biol. 296*, 899−910.
23. Stone, D., and Smillie, L. B. (1978) The amino acid sequence of rabbit skeletal α-tropomyosin. The NH_2-terminal half and complete sequence. *J. Biol. Chem. 253*, 1137−48.
24. Naraghi, M. (1997) T-jump study of calcium binding kinetics of calcium chelators. *Cell Calcium 22*, 255−68.
25. Felts, A. K., Gallicchio, E., Wallqvist, A., and Levy, R. M. (2002) Distinguishing native conformations of proteins from decoys with an effective free energy estimator based on the OPLS all-atom force field and the surface generalized Born solvent model. *Proteins 48*, 404−22.
26. Liu, Y., and Beveridge, D. L. (2002) Exploratory studies of ab initio protein structure prediction: Multiple copy simulated annealing, AMBER energy functions, and a generalized Born/solvent accessibility solvation model. *Proteins 46*, 128−46.
27. Christensen, I. T., and Jorgensen, F. S. (1997) Molecular mechanics calculations of proteins. Comparison of different energy minimization strategies. *J. Biomol. Struct. Dyn. 15*, 473−88.
28. Sale, K., Sár, C., Sharp, T. A., Hideg, K., and Fajer, P. G. (2002) Structural determination of spin label immobilization and orientation: A Monte Carlo minimization approach. *J. Magn. Reson. 156*, 104−12.
29. Huang, E. S., Ram Samudrala, R., and Ponder, J. W. (1999) Ab initio fold prediction of small helical proteins using distance geometry and knowledge-based scoring functions. *J. Mol. Biol. 290*, 267−81.
30. Heeley, D. H., Golosinska, K., and Smillie, L. B. (1987) The effects of troponin T fragments T1 and T2 on the binding of nonpolymerizable tropomyosin to F-actin in the presence and absence of troponin I and troponin C. *J. Biol. Chem. 262*, 9971−8.
31. Brittain, H. G., Richardson, F. S., and Martin, R. B. (1976) Terbium (III) emission as a probe of calcium (II) binding sites in proteins. *J. Am. Chem. Soc. 98*, 8255−60.
32. Martin, R. B., and Richardson, F. S. (1979) Lanthanides as probes for calcium in biological systems. *Q. Rev. Biophys. 12*, 181−209.
33. Kilhoffer, M.-C, Demaille, J. G., and Gerard, D. (1980) Terbium as luminescent probe of calmodulin calcium-binding sites: Domains I and II contain the high-affinity sites. *FEBS Lett. 116*, 269−72.
34. Ortiz, A. R., Kolinski, A., and Skolnick, J. (1998) Nativelike topology assembly of small proteins using predicted restraints in Monte Carlo folding simulations. *Proc. Natl. Acad. Sci. U.S.A. 95*, 1020−5.
35. Gibbs, N., Clarke, A. R., and Sessions, R. B. (2001) Ab initio protein structure prediction using physicochemical potentials and a simplified off-lattice model. *Proteins 43*, 186−202.
36. Ishikawa, K., Yue, K., and Dill, K. A. (1999) Predicting the structures of 18 peptides using Geocore. *Protein Sci. 8*, 716−21.
37. Jones-Hertzog, D. K., and Jorgensen, W. L. (1997) Binding affinities for sulfonamide inhibitors with human thrombin using Monte Carlo simulations with a linear response method. *J. Med. Chem. 40*, 1539−49.

38. Åqvist, J., Medina, C., and Samuelsson, J. E. (1994) A new method for predicting binding affinity in computer-aided drug design. *Protein Eng. 7*, 385−91.
39. Sham, Y. Y., Chu, Z. T., Tao, H., and Warshel, A. (2000) Examining methods for calculations of binding free energies: LRA, LIE, PDLD-LRA, and PDLD/S-LRA: Calculations of ligands binding to an HIV protease. *Proteins 39*, 393−407.
40. Potter, J. D., and Gergely, J. (1974) Troponin, tropomyosin, and actin interactions in the Ca^{2+} regulation of muscle contraction. *Biochemistry 13*, 2697−703.
41. Johnson, J. D., Jiang, Y., and Rall, J. A. (1999) Intracellular EDTA mimics parvalbumin in the promotion of skeletal muscle relaxation. *Biophys. J. 76*, 1514−22.
42. Blum, H. E., Lehky, P., Kohler, L., Stein, E. A., and Fischer, E. H. (1977) Comparative properties of vertebrate parvalbumins. *J. Biol. Chem. 252*, 2834−8.
43. Cates, S. M., Berry, M. B., Ho, E. L., Li, Q., Potter, J. D., and Phillips, G. N., Jr. (1999) Metal-ion affinity and specificity in EF-hand proteins: coordination geometry and domain plasticity in parvalbumin. *Structure 7*, 1269−78.
44. Müntener, M., Käser, L., Weber, J., and Berchtold, M. W. (1995) Increase of skeletal muscle relaxation speed by direct injection of parvalbumin cDNA. *Proc. Natl. Acad. Sci. U.S.A. 92*, 6504−8.
45. Resetar, A. M., Stephens, J. M., and Chalovich, J. M. (2002) Troponin-tropomyosin: an allosteric switch or a steric blocker? *Biophys. J. 83*, 1039−49.
46. Kraulis, P. J. (1991) MOLSCRIPT: A program to produce both detailed and schematic plots of protein structures. *J. Appl. Crystallogr. 24*, 946−50.
47. Merritt, E. A., and Bacon, D. J. (1997) Raster3D photorealistic molecular graphics. *Methods Enzymol. 277*, 505−24.

BI035067O